SOME BASIC MEASUREMENTS FOR ANALYSIS OF ELECTROSTATIC DUST PRECIPITATION

Thesis for the Degree of Ph. D.
MICHIGAN STATE UNIVERSITY
Ross Deline Brazee
1957

This is to certify that the

thesis entitled

Some Basic Measurements for
Analysis of Electrostatic
Dust Precipitation

presented by

Ross D. Frazee

has been accepted towards fulfillment
of the requirements for

Ph. D. degree in Agricultural Engineering

Wesley F Buchele
Major professor

Date September 19, 1957

SOME BASIC MEASUREMENTS FOR ANALYSIS OF ELECTROSTATIC DUST PRECIPITATION

By

Ross Deline Brazee

AN ABSTRACT

Submitted to the School for Advanced Graduate Studies of
Michigan State University of Agriculture and
Applied Science in partial fulfillment of
the requirements for the degree of

DOCTOR OF PHILOSOPHY

Department of Agricultural Engineering

Year 1957

Approved Wesley F. Buchele

ROSS DELINE BRAZEE AN ABSTRACT

Fundamental information has been developed for eventual application to the design of dust application methods and equipment. Specific areas investigated were: the corona discharge between concentric cylinders, size distributions of dust particles, determination of electrical charge on dust, and analysis of dust precipitation in a cylindrical field.

A study was made of three analytical expressions relating the current and voltage for a corona discharge in air between two concentric cylinders in terms of ionic mobility and cylinder geometry. The most satisfactory equation was applied in an indirect experimental method of measuring ionic mobility. The observed decrease of ionic mobility with increase in humidity, differences in positive and negative ion mobilities, and gas density influences on ionic mobilities were explained on the basis of modern gaseous electronics.

The log-normal frequency distribution was shown to describe experimentally determined particle-size distributions.

An analytical method of predicting total (maximum) charge per unit mass of dust was developed for a concentric-cylinder ionizing charger. An experimental charge-measurement method was also devised. The methods were compared exper-

imentally and found to be satisfactory. Disagreement in measured and calculated results was concluded to arise from lowered ionic mobilities in the dust-laden inter-electrode atmosphere.

The usefulness of the techniques developed was illustrated through a simple analysis of dust precipitation in a cylindrical electric field. It was shown that high but not impractical potentials, would be necessary to overcome the strong influences of air currents.

SOME BASIC MEASUREMENTS FOR ANALYSIS OF ELECTROSTATIC DUST PRECIPITATION

By

Ross Deline Brazee

A THESIS

Submitted to the School for Advanced Graduate Studies of Michigan State University of Agriculture and Applied Science in partial fulfillment of the requirements for the degree of

DOCTOR OF PHILOSOPHY

Department of Agricultural Engineering

Year 1957

Ross Deline Brazee

candidate for the degree of

Doctor of Philosophy

Final Examination, September 19, 1957, 9:30 A.M., Room 218, Agricultural Engineering Building

Dissertation: Some Basic Measurements for Analysis of Electrostatic Dust Precipitation

Outline of Studies

Major Subject: Agricultural Engineering
Minor Subjects: Physics, Mathematics

Biographical Items

Born, October 9, 1930, Adrian, Michigan

Undergraduate Studies, Michigan State University, 1948-1952

Graduate Studies, Michigan State University, 1952-1953, cont. 1955-1957

Experience: Graduate Assistant, Michigan State University, 1952-1953: Instructor, Michigan State University, 1955; Graduate Assistant, Michigan State University, 1955-1957.

Member of Tau Beta Pi, Pi Mu Epsilon, Sigma Pi Sigma, Society of the Sigma Xi, American Society of Agricultural Engineers.

TABLE OF CONTENTS

LIST OF TABLES

LIST OF FIGURES

ACKNOWLEDGMENTS

Many individuals assisted in making possible the work reported herein.

Dr. A.W. Farrall, Head of the Agricultural Engineering Department, made available the research assistantship.

The Rackham Foundation and Corn States Hybrid Service provided financial support.

Dr. Wesley F. Buchele, Agricultural Engineering Department, as major professor continually provided guidance and encouragement.

Dr. Donald J. Montgomery, of the Physics Department, contributed many hours of guidance in experimentation and analysis.

Drs. Carl W. Hall and Merle L. Esmay, Agricultural Engineering Department, and Dr. Edward A. Nordhaus, Mathematics Department, served as guidance committee members.

Dr. Walter M. Carleton, formerly of the Agricultural Engineering Department and now with the Agricultural Engineering Research Division, United States Department of Agriculture, guided the early phases of the work.

Dr. C. D. Hause of the Physics Department furnished some apparatus for the studies.

Mr. James Cawood and the staff of the Agricultural Engineering Research Laboratory gave helpful assistance

in construction of apparatus.

Mr. Ronald Hamelink, Mr. Howard Wilson and Mr. Glen Vandenberg gave valuable assistance in instrumentation, experimental work and analysis of data. Mr. Scott Hedden helped with the photographic work.

The author expresses most sincere appreciation to these individuals and all others who assisted in any way.

The author also extends thanks to his wife, Mrs. Jean Roth Brazee, for her endurance and encouragement, and for typing this thesis.

INTRODUCTION

Control of plant diseases and insects is of great concern to the farmer and urban dweller alike. Fracker and others (1954) estimate that the average annual crop losses over the period 1942-1951 amounted to about 3 billion dollars from plant diseases, and about one billion dollars from insect infestations. These figures included field and forage crops, fruit and nut crops, vegetable crops, drug crops and ornamental plants. This loss results in a reduction in the quantity and quality of produce available to the consumer, as well as a drain on producer income.

Fracker's estimates include all losses whether or not they arise from causes that are preventable with present technical knowledge. The magnitude of the losses raises doubt that present means of insect and disease control are being efficiently used.

Chemical preparations are important for pest and disease control. Smith and others (1954) estimate that in the United States, in 1952, about 2½ million acres were dusted or sprayed an average of 2.86 times, at a total cost of about 193 million dollars. This cost emphasizes the importance of efficient pesticide application to ensure that the investment in control is not a loss.

Dusting is an often used, convenient application method, but it is susceptible to loss of pesticidal material through drifting of the dust cloud. Bowen (1951) and Ban (1955) found that only ten to twenty percent of the pesticide delivered by a conventional machine reaches the plants.

The Michigan State University pesticide-application study was undertaken in 1950 to determine the fundamentals of dust precipitation and thereby provide the basis for improving deposition efficiency.

Background of the Study

The work was begun with a study of electrostatic dust precipitation by Bowen (1951) and Hebblethwaite (1952), who found that Rampe (1947) and others of France had some success with the method.

A dust charging "nozzle" in the form of a cylindrical condenser was used. Aerosol particles picked up air ions as they passed through the intense field of the nozzle. The potential gradient of the resulting charged cloud was used to drive the particles onto the plant.

Although one hundred percent improvement of depositing efficiency was obtained in some cases, the method was not always successful. Hebblethwaite found that its effectiveness fell off with increasing relative humidity. Brazee (1953) reported that electrical breakdown of incidental nozzle coatings of certain dusts also hindered charging.

Brittain (1954) made experiments on the effects of depositing surfaces upon dust recovery. An important result was that high aerosol stream velocities tended to decrease recovery of coarser dusts. He attributed this to an erosion effect of the aerosol stream. Recovery of dust was greater for more pubescent and prominently veined leaves.

Mathematical and experimental studies by Bowen (1953) showed that assumption of a continuous charge distribution for theoretical analysis was justified. Using this fact, Bowen and Splinter (1955) began a study of dust precitation forces.

Inertial forces, arising from deflection of the aerosol stream by the precipitation surface, and electrical forces were considered in theory and experiment. Inertial forces were found highly significant, especially for large particles. The only electrical forces considered were those occurring naturally owing to a charge distribution. Since they depended upon the electric field configuration, they were sometimes as important as inertial forces; in other cases they were negligible. In the case of very small particles (less than 2 microns radius), it was concluded that electrical forces exerted the only significant effect for useful deposition.

In field tests, Ban found that leaves in the outer regions of bean plants had heavier deposits when charged dust was used. However, the recovery for the inner

regions (termed hidden leaves) was greater for uncharged dust. He attributed this to reflection of the aerosol stream from the soil surface into the hidden leaf region.

Laboratory tests were made by Ban to study the effect of an applied electric field upon precipitation of a number of dusts. The field was supplied by a plane charged screen, having the same charge polarity as the dust. Favorable effects were noted in many, but not all, cases. Finer dusts appeared to receive greater benefit.

At the beginning of the studies of this thesis, then, the groundwork had been laid for continued theoretical and experimental study of particle precipitation forces, including externally applied electric fields.

Statement of the Problem in the Present Work

It was decided that the most fruitful areas of investigation for this work would be: the concentric-cylinder corona discharge and its behavior with variations in relative humidity, analytical description of dust particle size distributions, and determination of electrical charge on dust. These findings, as well as those of previous workers, will be applied to an analysis of dust precipitation in a cylindrical electric field.

AN EXPERIMENTAL STUDY OF THE CORONA DISCHARGE CHARACTERISTICS OF A WIRE IN A COAXIAL CYLINDER

A study of the corona discharge characteristics of a fine wire coaxial with respect to a grounded metal cylinder was undertaken. An analytical expression between current and voltage for given ion mobility and cylinder geometry was desired for design of experimental dust chargers, and information was needed about ionic mobilities and the influences of atmospheric humidity and air velocity upon the corona discharge.

Review of Literature

Parsons (1924) derives an equation intended to express the current-voltage relation in the corona discharge between a cylinder and a coaxial wire. Under such circumstances almost all ionization occurs within a small region surrounding the wire. Outside this region the charge carriers are ions of the same electrical sign; i.e., for a positive wire potential, negative ions move toward the wire while the positive ions leave the ionization region and travel outward to the grounded cylinder. In the derivation Parsons accounts for expansion of the ionization region as voltage increases. The final form of Parsons' equation is

$$i = CV(V-V_o)/(V_1-V), \qquad (1)$$

where i is the current per unit wire length; V is the applied wire voltage; V_o is the voltage necessary to start the corona, and

$$C = 2kr_o/R^2\beta , \tag{2}$$

and

$$V_1 = (r_o/\beta)\ln(R/r_o) + V_o. \tag{3}$$

Here k is the ionic mobility (the velocity of an ion in a field of unit strength); r_o is the wire radius; R is the cylinder radius; β is the rate of increase of the corona region radius, r_i, with respect to applied potential, that is,

$$r_i = r_o + \beta(V-V_o). \tag{4}$$

Experimental Investigation

An experiment was made to obtain corona-discharge current-voltage data. The tests included several sizes of wires and cylinders, and extended over a range of relative humidities. The effect of variation in the velocity of air movement through the tube was also studied. The effect of an aerosol in the stream was not taken up in this experiment.

The equipment was set up in a laboratory chamber for humidity control, as shown in Figure 1. Figure 2 shows the test stand holding the cylinder-wire combination under test. Clamps were provided for holding the grounded aluminum-tubing cylinders. Plexiglas insulators held the corona wire in proper position at the cylinder's longitudinal axis.

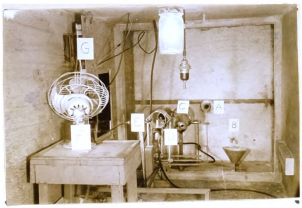

Figure 1. Experimental apparatus for the corona discharge investigation.

A. Air circulation outlet.

B. Steam outlet for high humidity tests.

C. Variable speed fan.

D. Cylinder and wire stand.

E. Air velocity probe.

F. Fan for air circulation over wet and dry bulb thermometers (G) for relative humidity measurement.

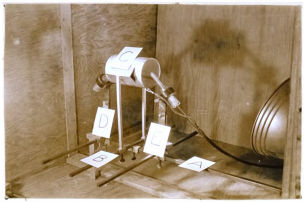

Figure 2. The cylinder-wire test stand.

A. Base.

B. Mounting rails.

C. Cylinder clamps with section of aluminum tubing in place.

D and E. Mounting brackets for Plexiglas connectors between which wire was stretched along cylinder axis.

The direct current potential was obtained through electronic voltage-tripler circuits, one of positive and the other of negative polarity so that both discharges could be studied.

Air movement through the cylinder was controlled by using a variable-speed centrifugal fan, and velocity was measured by means of a Hastings hot-wire anemometer. The meter probe was mounted on a traversing lever actuated by a solenoid, which allowed positioning of the probe for measurements without disturbing the chamber atmosphere.

Table 1 shows the tube and wire size combinations, air velocities, temperatures and relative humidities for which current-voltage data were taken.

Parsons' equation was written in the form

$$iV_1 + VD - V^2C = iV, \tag{5}$$

where

$$D \equiv CV_o. \tag{6}$$

The quantities V_1, V_o, and C were taken as parameters for adapting Parson's equation (1) to a set of i and V values taken at a specific polarity and humidity. Fluctuations were smoothed by plotting the data on logarithmic coordinates and fitting a straight line. Three i-V pairs were selected from the plot and inserted in equation (5), giving three algebraic equations that were solved for V_1, V_o, and C.

TABLE 1.

TUBE AND WIRE SIZE COMBINATIONS, AIR VELOCITIES, TEMPERATURES AND RELATIVE HUMIDITIES FOR WHICH CORONA DISCHARGE CURRENT-VOLTAGE DATA WERE TAKEN.

Average Air Velocity (ft./min.)	R	r_o x 10^2	Positive Corona						Negative Corona					
			Low*		Medium*		High*		Low		Medium		High	
	(cm.)	(cm.)	t**	R.H. ***	t	R.H.	t	R.H.	t	R.H.	t	R.H.	t	R.H.
500	1.90	6.82	81.5	21	96.3	64	91.6	92	92.0	30	96.8	64	92.5	98
500	1.90	0.635	86.2	42	82.3	65	103.1	97	85.5	42	83.2	63	102.7	96
500	2.38	1.50	72.5	32	75.3	63	108.5	93	71.7	32	75.3	59	108.5	95
1000 to 2000	3.65	2.87	94.0	27	97.0	61	112.0	96	94.7	23	97.0	59	112.4	94
1000	3.65	0.635	93.4	36	95.7	61	105.6	97	93.3	36	94.1	63	106.1	97
1000	4.92	6.82	82.5	37	85.6	60	****	****	83.8	35	85.8	60	****	****
1000	4.92	1.50	89.0	36	94.8	60	106.7	93	88.3	41	95.1	58	107.1	93
1000	4.92	0.635	84.6	38	87.5	61	101.8	96	84.7	38	88.8	58	101.4	96

* Humidity level.
** Dry-bulb temperature (^oF).
*** Percent relative humidity.
**** These data were not obtainable owing to failure of the particular combination to function at high humidity.

The constant β was then determined by solving equation (3):

$$\beta = r_o \ln(R/r_o)/(V_1 - V_o). \qquad (7)$$

The apparent ionic mobility k was given by equation (2) in the form

$$k = CR^2\beta/2r_o. \qquad (8)$$

Discussion of Results

Numerical results are tabulated in Table I of Appendix A, and ionic mobilities are plotted against relative humidity in Figures 3 and 4.

Trial calculations, which are not presented, showed that Parsons' equation would be fairly suitable as a design equation.

In practically all instances the apparent ionic mobility was observed to decrease as relative humidity increased. An examination of the individual points plotted indicates that in many cases the mobilities decreased less rapidly at high humidity. The negative-ion mobilities were in general slightly higher than the positive. There was some tendency for the mobilities to run higher for the smaller wire diameters. The measured ionic mobilities in air are of the same order as values quoted in modern work, e.g., in von Engel (1955) and in Loeb (1955). The experimental error in the ionic mobilities was estimated to be about $\pm$ 9 percent.

Reynolds number calculations showed that the air flow was turbulent in all cases. The ratio of the transverse to the longitudinal ionic drift velocity (with respect to the cylinders)

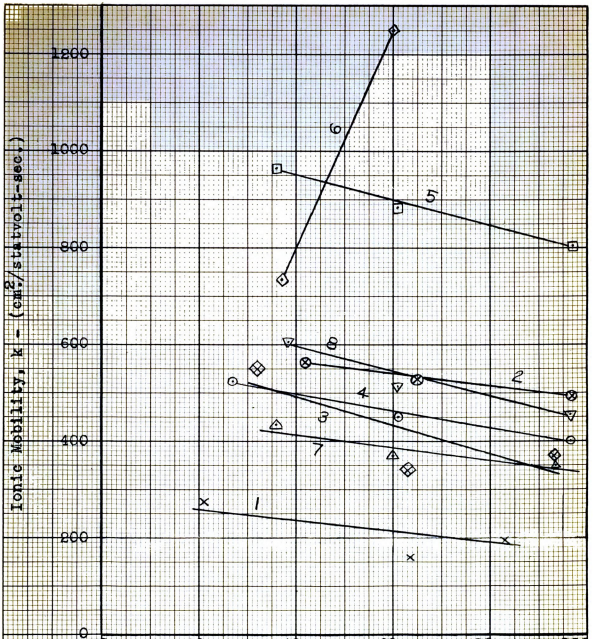

Figure 3. The effect of atmospheric relative humidity on the mobility of positive air ions. See page 14 for an explanation of the coding symbols.

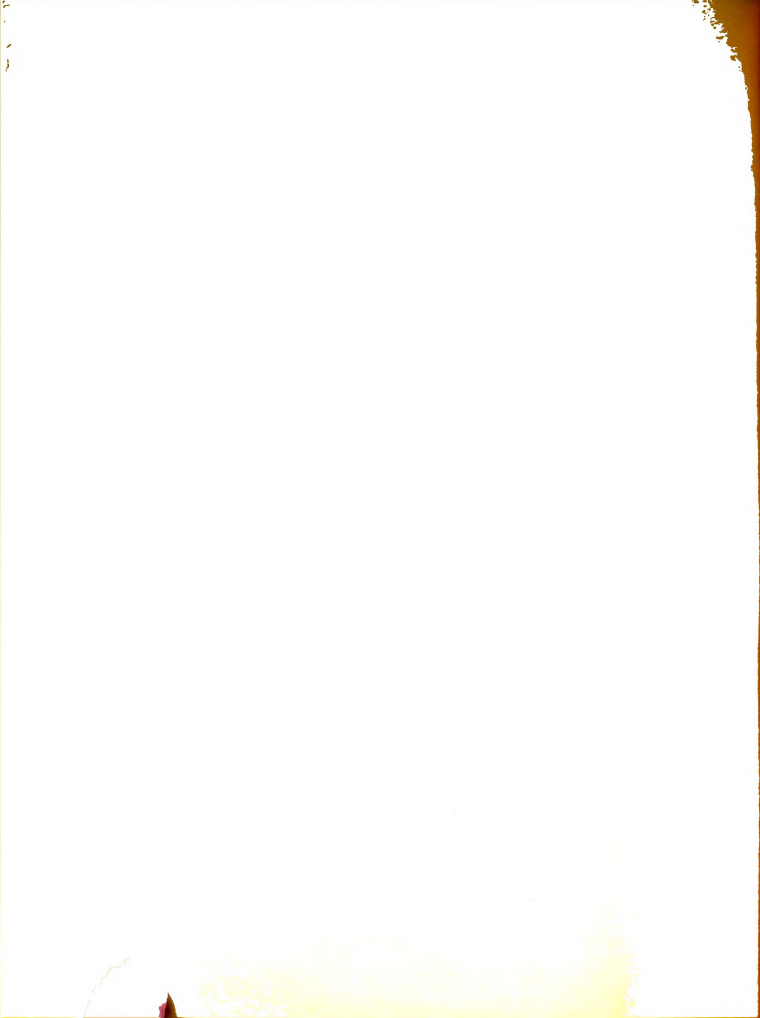

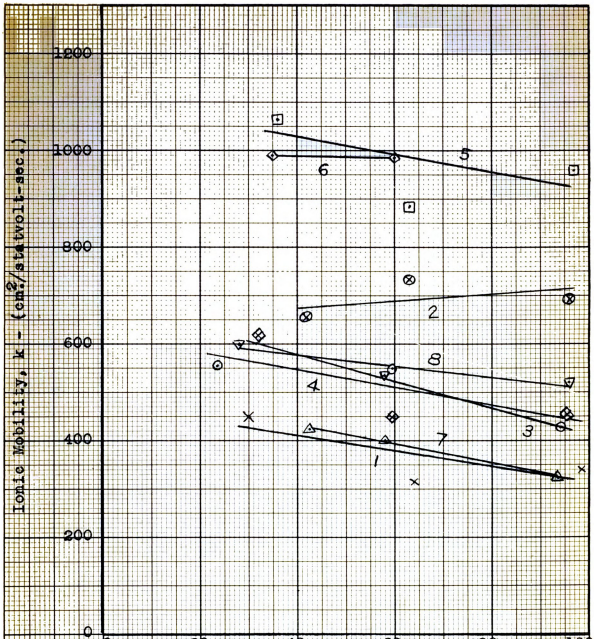

Figure 4. The effect of atmospheric relative humidity on the mobility of negative air ions. See page 14 for an explanation of the coding symbols.

Explanation of Symbols Used in Figures 3 and 4.

Test and Curve Number	Symbol for Individual Points	R (cm.)	r_o x 10^2 (cm.)
1	×	1.90	6.82
2	⊗	1.90	0.635
3	◈	2.38	1.50
4	⊙	3.65	2.87
5	⊡	3.65	0.635
6	◈	4.92	6.82
7	◬	4.92	1.50
8	▽	4.92	0.635

varied from about 2.54×10^{-2} to 0.96. Under these conditions no significant effects on the corona owing to air movement were noted with the instrumentation employed.

It is important to note that constant temperature could not be maintained with varying humidity, as Table 1 shows, owing to the characteristics of the control system.*

Conclusions

The experimental method used is convenient from the standpoint of simplicity in apparatus requirements. The amount of computation in solving the algebraic equations is a disadvantage when treating a large volume of experimental data.

Substantial refinement of technique and instrumentation would be necessary to reduce the experimental error. In particular, a well-regulated power supply would be important in maintaining steady readings. The humidity-control system should allow for more exact temperature regulation, since temperature fluctuation may be a major cause of erratic results.

More recent work with the method shows consistent appearance of a slight curvature of a logarithmic plot of the current-voltage data. Hence, it is perhaps an over-simplification to represent these data by a straight line.

Detailed discussion of the ionic-mobility results will be reserved for the section of this thesis immediately following.

---

*The reader is referred to Brittain (1954) for a detailed description of the system.

DISCUSSION OF THE CONCENTRIC-CYLINDER CORONA DISCHARGE AND IONIC MOBILITY

Two additional current-voltage expressions for the concentric cylinder discharge will be presented and compared with Parsons' equation (1). A critical corona-gradient* equation for the same discharge will be considered.

The experimental ionic-mobility results of the preceding section will also be discussed in the light of modern gaseous electronics.**

The Concentric-Cylinder Corona Discharge

Current-Voltage Equations. In discussing the current-voltage relationship von Engel (1955) states a criterion for taking space charge into account in deriving the electric potential distribution between concentric cylinders: when the space charges between the cylinders become of the same order as the surface charges on the electrodes, space charge must be considered. With ρ the constant space-charge density, V the inner cylinder potential (the outer cylinder grounded)

---

* The critical corona gradient is the electric field strength, at $r=r_0$, at which corona discharge starts.

** The term gaseous electronics refers to the physics of electrical discharges in gases.

and C the capacitance per unit length, the criterion is mathematically

$$\rho \cdot \text{volume} \simeq VC, \tag{9}$$

or, in the notation of the preceding section,

$$\rho \pi R^2 \simeq V/2 \ln(R/r_o). \tag{10}$$

For example, with V = 12 statvolts, $r_o = 2 \times 10^{-2}$ cm., R= 1 cm, $\ln(R/r_o) \simeq 4$, space charge may be expected to have notable influence when $\rho \simeq 0.5$ statcoulomb/cm.^{3}, or when the number of elementary charges $N \simeq 10^9$ charges/cm.^{3}

Von Engel proceeds with his derivation using Poisson's equation. The current-voltage expression which results is very complicated. Therefore von Engel assumes that $R(2i/k)^{\frac{1}{2}} \ln(R/r_o)/V_o \ll 1$, and he obtains approximately

$$i = kV_o(V-V_o)/R^2 \ln(R/r_o), \tag{11}$$

in the notation of the previous section. He further comments that when $V \gg V_o$, empirically $i \propto V(V-V_o)$, rather than $V_o(V-V_o)$. For radii $r \gg r_o$, the electric field intensity vector $\bar{E}$ is given by

$$\bar{E} = (2i/k)^{\frac{1}{2}} \bar{r}/r. \tag{12}$$

The conditions of the corona tests of this thesis do not satisfy the approximations made in deriving equation (11). Therefore it is impossible to evaluate the suitability of equation (11) on the basis of the experimental data.

Cobine (1941) and Thomson and Thomson (1933) give the theoretical current-voltage relation

$$i = 2kV(V-V_o)/R^2 \ln (R/r_o). \tag{13}$$

A similar equation is also deduced by Parsons (1924), but it is modified into the form of his equation (1).

Equation (13) may be written in the form

$$V = \left[R^2 \ln(R/r_o)/2k\right](1/V) + V_o. \qquad (14)$$

Equation (14) predicts that a plot of V against 1/V will yield a straight line, permitting evaluation of k and V_o. This procedure may be illustrated with the data of Test No. 7, for positive corona, listed in Table I of Appendix A. The results for k and V_o from equation (13) and those from Parsons' equation (1) appear in Table 2. Ionic mobility is plotted against relative humidity, for both equations, in Figure 5.

TABLE 2.

IONIC MOBILITIES (k) AND CORONA STARTING VOLTAGES (V_o) GIVEN BY EQUATIONS (1) AND (13) FROM DATA OF TEST NO. 7, POSITIVE CORONA, TABLE I OF APPENDIX A

Percent Relative Humidity	Equation (1)		Equation (13)	
	V_o*	k**	V_o	k
36	7.16	434	9.30	1210
60	5.86	371	9.40	934
93	6.58	352	10.0	815

*V_o is given in kilovolts.

**k is given in cm.^{2}/statvolt-sec.

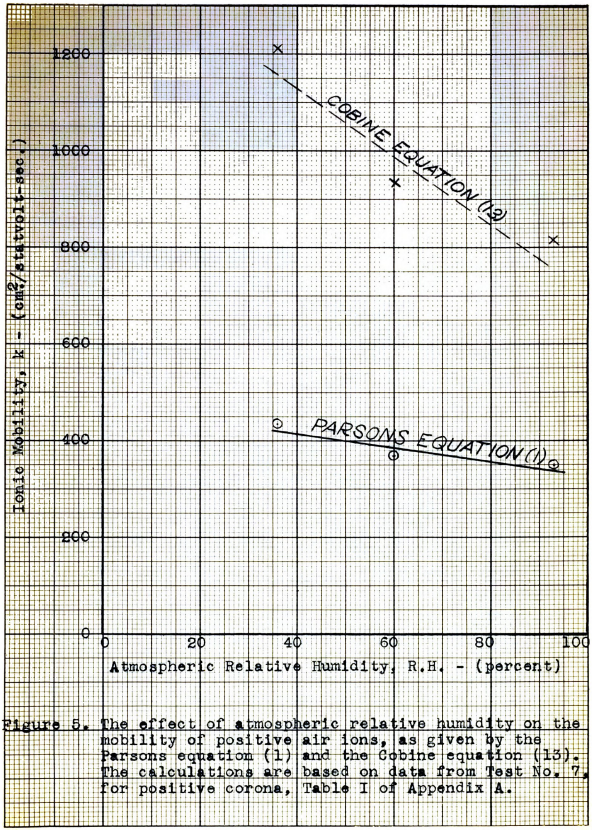

Figure 5. The effect of atmospheric relative humidity on the mobility of positive air ions, as given by the Parsons equation (1) and the Cobine equation (13). The calculations are based on data from Test No. 7, for positive corona, Table I of Appendix A.

Equation (13) yields results for k about 2.5 times the acceptable values given by Parsons' equation (1).

Equation (1) may be written

$$1/C = V(V-V_o)/i(V_1-V), \qquad (15)$$

and equation (13) may be stated as

$$R^2 \ln (R/r_o)/2k = V(V-V_o)/i. \qquad (16)$$

If $V(V-V_o)$ is plotted against $i(V_1-V)$ for equation (15), and $V(V-V_o)$ against i for equation (16), straight lines intercepting the origins should be obtained. Figures 6 and 7 show that this is essentially true on the basis of data from Test No. 7, positive corona, Table I of Appendix A. Equation (15) departs from the straight line at higher values of $V(V-V_o)$ and $i(V_1-V)$.

Figure 7 indicates that an equation of the form $i \propto V(V-V_o)$, such as (13), represents the current-voltage relation. The mobility results, however, give evidence that the proportionality is probably over-simplified.

Meek and Craggs (1953), Loeb, and von Engels discuss the atomic and molecular processes in electrical discharges at considerable length. Photoionization, recombination, attachment and detachment, ionization and excitation by impact and light emission are among the processes known to occur. These will not be taken up here, but they are mentioned to point out the complexity of the electrical discharge. This complexity is a barrier to the development of more adequate theory than the foregoing.

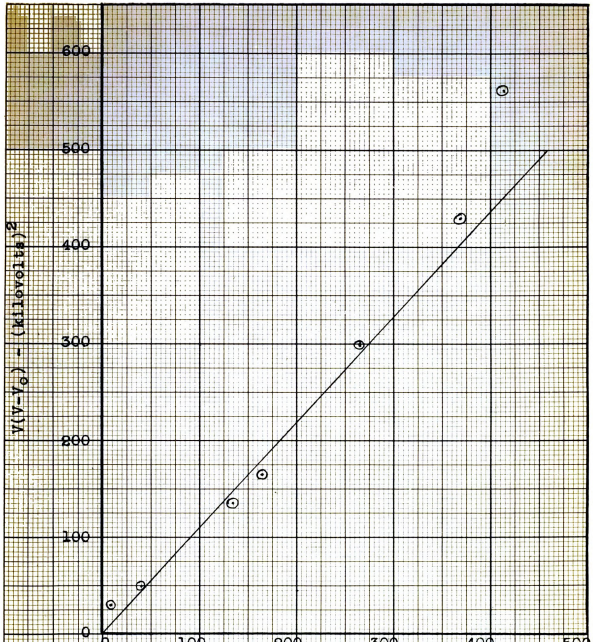

Figure 6. A plot of equation (15) to show the applicability of the Parsons equation (1). The experimental data used were from Test No. 7, positive corona, 36 percent relative humidity, of Table I of Appendix A.

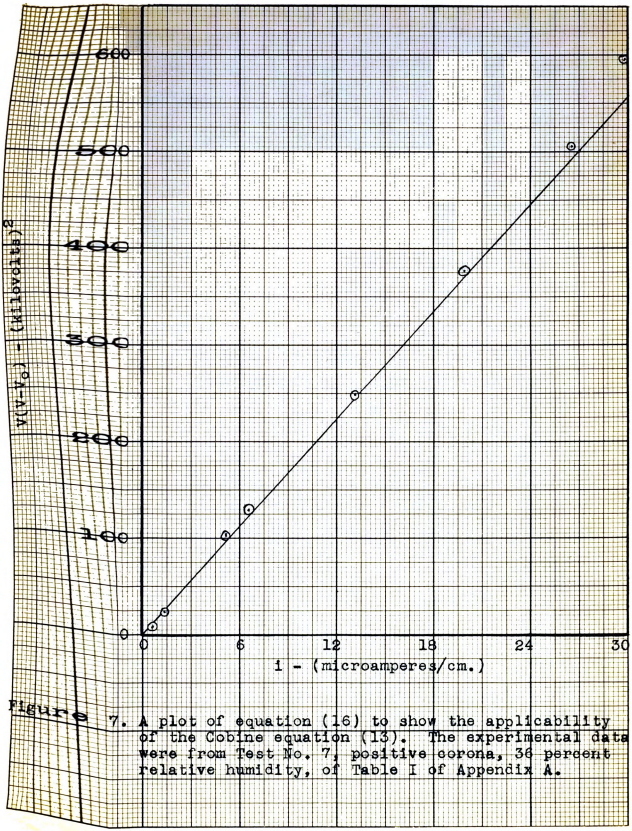

Figure 7. A plot of equation (16) to show the applicability of the Cobine equation (13). The experimental data were from Test No. 7, positive corona, 36 percent relative humidity, of Table I of Appendix A.

The Critical Corona Gradient. Cobine, and Thomson and Thomson, give a semi-empirical equation for the electric field strength E_o at the inner cylinder $r = r_o$ necessary to start the corona:

$$E_o = 30 + 9/(r_o)^{\frac{1}{2}} \text{ (kv./cm.)}. \qquad (17)$$

Then V_o will be given by

$$V_o = E_o r_o \ln(R/r_o). \qquad (18)$$

Von Engel states that in the absence of a theory of breakdown in non-uniform fields it is impossible to calculate V_o and E_o from atomic data, and implies that experimental determination is the only approach at present. He cautions that accuracy of measurement of V_o is restricted by its dependence upon surface roughness and chemical composition of the wire, as well as the polarity.

Consideration of the Measured Ionic Mobilities of the Corona Discharge Experiment

The relation between the drift velocity v of an ion through a gas in the field direction and the field strength E defines the mobilities k through

$$v = kE. \qquad (19)$$

To obtain a satisfactory theoretical expression for the ionic mobility k which would allow its calculation from atomic and molecular data is very difficult. Relationships have been derived on the basis of classical kinetic theory, but their predictions always disagreed with observed facts in

some manner. In recent years workers in gaseous electronics have attacked the problem with quantum theory and with modern measuring techniques, but no generalized theory has been advanced. Consequently the following discussion will be largely qualitative.

Influence of Humidity Upon Mobilities. Experimentally, the apparent ionic mobility for air decreased as relative humidity increased (see Figures 3 and 4).

Tyndall (1938) attributes this effect to the polar nature of water molecules. Loeb found that the presence of polar impurities prompted formation of clustered or complex ions. Sometimes the complex ions are of a charge specific nature, meaning that a specific chemical reaction takes place. Loeb states that the mobility may decrease or increase depending upon the gas and impurities.

Apparently, in the case of water vapor in air, the cluster ions have sufficiently large collision radii to effectively lower the apparent ionic mobility.

The Effect of Gas Density on Mobility. The corona discharge experiments of this thesis were carried out under essentially constant pressure conditions of 1 atmosphere. Since temperature was not held constant, variations in air density occurred. The ratio of gas densities ρ_2/ρ_1 is

$$\rho_2/\rho_1 \simeq T_1/T_2, \qquad (20)$$

where T_1 and T_2 are the absolute temperatures. The density variations are summarized in Table 3, based on the temperature

TABLE 3.

AIR DENSITY VARIATIONS IN THE CORONA DISCHARGE EXPERIMENT.

R	r_o x10^2	Air Density Ratios							
		Positive Corona				Negative Corona			
(cm.)	(cm.)	R.H.*	ρ_2/ρ_1^{**}	R.H.	ρ_3/ρ_1^{**}	R.H.	ρ_2/ρ_1	R.H.	ρ_3/ρ_1
1.90	6.82	64	0.974	92	0.983	64	0.990	98	0.996
1.90	0.635	65	1.010	97	0.968	63	1.00	96	0.972
2.38	1.50	63	0.997	93	0.937	59	0.993	95	0.933
3.65	2.87	61	0.997	96	0.969	59	0.997	94	0.969
3.65	0.635	61	0.993	97	0.977	63	0.997	97	0.977
4.92	6.82	60	0.993	****	****	60	0.997	****	****
4.92	1.50	60	0.990	93	0.968	58	0.987	93	0.965
4.92	0.635	61	0.993	96	0.968	58	0.990	96	0.968

* Percent relative humidity.

** Air density at medium humidity level ÷ air density at low humidity level of given test (taken to be unity).

*** Air density at high humidity level ÷ air density at low humidity level.

**** Data were not available.

data of Table 1.

Loeb states that k is inversely proportional to the density of gas molecules. In the light of this, comparison of Table 3 with the mobility plots of Figures 3 and 4 may explain (within experimental error) the smaller rate of decrease of mobility with respect to humidity at higher humidities noted in most of the experiments. In such cases the air density at the high humidity level is usually appreciably less than that at the low and medium levels.

Differences in Mobilities of Positive and Negative Ions. Negative ion mobilities were found to be higher than the positive. These results are in agreement with those of other experimenters.

Loeb describes the "aging" effect which contributes to this mobility difference. He mentions experiments with room air, where initial positive ions had the same elevated mobility difference. He mentions experiments with room air, where initial positive ions had the same elevated mobility of 1.8 $cm.^2$/volt-sec. as the negative ions. However, if the positive ions aged for a few hundredths of a second, their mobility changed sharply to the normally observed value of 1.4 cm^2/volt sec. Apparently the mobility change took place in a single act of addition in much less than 10^{-2} second. Experiments show that in dry air the aging process occurs in less than 1.4 milliseconds, and aging may be delayed by addition of water vapor. The amount of delay depends upon the

quantity of water vapor. From this one might expect the positive and negative mobilities to differ less in air of higher humidity.

Von Engel attributes the mobility difference in air to a strong tendency of oxygen molecules to attach electrons, whereas this does not occur for nitrogen molecules. As a result, sufficient electrons remain free to show a slightly elevated mobility.

The Variation in Mobility with the Corona Wire Radius. The results of the corona experiment showed a tendency for the mobilities to run higher for smaller wire radii (see Figures 3 and 4).

There seems to be no cause to expect this on the basis of present theory of gaseous electronics. It seems better to leave this phenomenon unexplained, since it may well arise from failure of Parsons' equation, with its purely classical character, to represent the true physical situation.

General Discussion. The agreement of the corona experiment findings with the results of others serves to bolster confidence in the work of this thesis.

The concentric cylinder discharge is an indirect method of mobility measurement; for more accurate measurements direct methods are recommended. Loeb discusses several direct methods of mobility measurement in considerable detail.

DUST PARTICLE SIZE DISTRIBUTIONS

Ban (1955) describes a method for sizing dust particles, using a microscope equipped with an ocular scale, and supplies results of particle size measurements for several ducts. The purpose of the following study was to find a concise method of describing the particle size distribution on the basis of such data.

Review of Literature

Dallavalle (1943) presents a semi-graphical method of analyzing size-frequency data, based upon the following theory:

Suppose that the size measurement data are divided into convenient size groups. A "size-frequency" curve is obtained by plotting percent frequency of various particles against the mean of size groups. Parameters other than the median or average particle sizes are necessary to define this distribution, when it is not of a standard form.

If F(D) is a function defining the frequency distribution of particles having diameters D_1, D_2, D_3,....*, and Q(D) is the sum of particles smaller (or greater) than a size D, then the number of particles between particles of

---

*The successive differences are considered infinitesimal.

diameters D_1 and D_2, is

$$q(D_1)-q(D_2) = \int_{D_2}^{D_1} F(D)dD \quad . \qquad (21)$$

The size-frequency curve, F(D), generally does not follow a normal distribution but rather a logarithmic-normal distribution.

The equation for the log-normal distribution is

$$F(D)=\left\{\sum n/\ln \sigma_g\left[(2\pi)^{\frac{1}{2}}D\right]\right\}e^{-(\ln D-\ln d_g)^2/2(\ln \sigma_g)^2}, \qquad (22)$$

where d_g is the geometric mean; σ_g is the geometric standard deviation, given by

$$\ln \sigma_g = \left\{\sum\left[n(\ln D-\ln d_g)^2\right]/\sum n\right\}^{\frac{1}{2}}. \qquad (23)$$

The constants d_g and σ_g completely define their corresponding frequency distributions.

The first step in applying the method is to calculate the cumulative percentage of particles below (or above) each size group. If these results give a straight line on logarithmic probability coordinates, the distribution is log-normal and equation (22) applies. In practice there are a smallest and a largest particle, whereas the grid requires the distributions to be asymptotic at both extremes. For this reason the plots may be expected to differ from the straight line at the extremes. It is permissible to overlook this because the areas extending from the extremes to infinity are negli-

ible compared with the area under the distribution curve between the largest and smallest particles measured.

The geometric mean particle diameter d_g is obtained by reading the size corresponding to 50 percent on the probability scale. The geometric standard deviation σ_g is

$$\sigma_g = 84.13 \text{ percent size}/50 \text{ percent size}$$
$$= 50 \text{ percent size}/15.87 \text{ percent size}. \quad (24)$$

Dallavalle indicates that in many cases 200 individual particle measurements, by microscope, are enough to give a representative sample.

Experimental Measurements

Table II of Appendix A presents the results of microscopic particle size measurements for three different dusts.

It was necessary to assume a priori that the log-normal distribution applied to Attasorb dust. The particle size ranges were excessively broad to give sufficient data for a conclusive plot. In all other cases a logarithmic probability plot fitted the data satisfactorily. A sample plot on logarithmic probability coordinates for CCC Diluent is given in Figure B of Appendix A. The values of d_g and σ_g for all dusts studied appear in Table III of Appendix A.

Conclusions

A limitation upon the accuracy of the particle size distribution is the resolving power of the microscope. In the experimental measurements (including those of Ban) sub-

stage illumination was used. Therefore, the resolving power z is

$$z = \lambda / \text{N.A.}, \qquad (25)$$

where λ is the wavelength of the illuminating light, and N.A. is the numerical aperture of the objective. A 43X objective with N.A. = 0.85 was used, and for λ = 5300 Angstroms, two lines separated by a distance of $z \simeq 0.6$ micron could be resolved. Hence, two particles whose adjacent surfaces are separated by a distance much less than z will be incorrectly taken as one larger particle. The resolving power in this situation can be increased by use of an oil immersion objective with substage illumination just sufficient to fill the aperture of the objective. Resolving power will be an important restriction when a large proportion of the particles have diameters not much greater than z.

The method of analyzing particle size frequency data is quite convenient, and the parameters thereby determined furnish an economical means of expressing the particle size distribution for a given dust. The particle size distribution of a given dust is necessary for theoretical analyses of the charging and dynamics of dust particles.

DETERMINATION OF ELECTRICAL CHARGE ON DUST

Knowledge of the magnitude of electrical charges on dust particles is important for evaluation of effectiveness of charging methods and for theoretical calculations. Methods for calculating and measuring electrical charge on dust were developed.

Theoretical Maximum Charge per Unit Mass of Dust Charged in a Concentric-Cylinder Corona Discharge

Ladenburg (1930) gives the maximum charge q_o attainable by a spherical particle of radius a in an electric field of intensity E as

$$q_o = E \left[3K/(K+2)\right] a^2, \qquad (26)$$

where K is the dielectric constant of the particle. Equation (26) holds provided $a > 0.5$ micron. E may be a function of position in the interelectrode space.

From equation (21), an element of charge per unit mass of dust, dQ_m, is given by

$$dQ_m = q_o F(D)\, dD \quad . \qquad (27)$$

Since $a = D/2$, and $F(D)$ is expressed by equation (22), equation (27) becomes

$$dQ_m = \frac{E\left[3K/(K+2)\right] D^2 N e^{-\left[\frac{(\ln D - \ln d_g)^2}{2(\ln \sigma_g)^2}\right]} dD}{4(2\pi)^{\frac{1}{2}} D \ln \sigma_g}, \qquad (28)$$

where $N = \sum n$ is the total number of particles of all diameters per unit mass of dust. Dallavalle (1943) gives an expression for N, based on the log-normal size distribution, of the form

$$\log N = -\left[\log (\epsilon \alpha_v) + 3 \log d_g + 10.362 (\log \sigma_g)^2\right], \quad (29)$$

where ϵ is the particle material mass density, and α_v is the volume shape factor. For spherical particles $\alpha_v = \pi/6$.

Equation (28) must be integrated over all particle diameters to obtain

$$Q_m = \int_0^\infty \frac{E\left[3K/(K+2)\right] d_g^2 \left(\frac{D}{d_g}\right)^2 N}{4(2\pi)^{\frac{1}{2}} \ln \sigma_g} e^{-\frac{1}{2(\ln \sigma_g)^2} \cdot \left(\ln \frac{D}{d_g}\right)^2} \frac{dD}{D}. \quad (30)$$

For convenience, let

$$B = E\left[3K/(K+2)\right] \cdot d_g^2 N / 4(2\pi)^{\frac{1}{2}} \ln \sigma_g, \quad (31)$$

and

$$s^2 = 1/2(\ln \sigma_g)^2. \quad (32)$$

Then

$$Q_m = B \int_{-\infty}^{\infty} e^{2 \ln(D/d_g)} \cdot e^{-s^2\left[\ln(D/d_g)\right]^2} d\left[\ln(D/d_g)\right]. \quad (33)$$

Upon writing $x = \ln(D/d_g)$, equation (33) becomes

$$Q_m = B \int_{-\infty}^{\infty} e^{-s^2x^2+2x} dx = B e^{1/s^2} \int_{-\infty}^{\infty} e^{-(sx-1/s)^2} dx = B e^{1/s^2} (\pi)^{\frac{1}{2}}/s. \quad (34)$$

From the definitions (31) and (32), we have finally,

$$Q_m = (1/4) E\left[3K/(K+2)\right] d_g^2 N e^{2(\ln \sigma_g)^2}. \quad (35)$$

We shall make use of Q_m in the following sense:

The total (maximum) charge ΔQ on an element of mass Δm large enough to contain many particles, but small enough that the electric field strength may be considered constant over it is given by

$$\Delta Q = Q_m \Delta m. \tag{36}$$

Lowe and Lucas (1953) state that charged dust particles, owing to their low mobility, have a space charge effect considerably greater than air ions. Lowe and Lucas give the electric field strength E between concentric-cylinder electrodes with dust present as

$$E = \frac{1}{r}\left[\left(\frac{1}{kp^2S^2} + C_o\right) e^{2pSr} - \frac{2i}{kpS}\left(r + \frac{1}{2pS}\right)\right]^{\frac{1}{2}}, \tag{37}$$

where $p = 3K/(K+2)$, S is the effective total surface area of dust per unit volume of air, and C_o is a constant of integration given by the condition

$$\int_R^{r_o} E \, dr = V, \tag{38}$$

where V is the applied voltage.

If $2pSr \ll 1$, as it is for the experiments herein considered, equation (37) may be simplified by expanding the exponential term, giving

$$E = \left[(2i/k)(1+2pSr/3)+C_o/r^2\right]^{\frac{1}{2}}. \tag{39}$$

Equation (39) will now be applied to estimating $q \equiv Q/m$, the total charge per unit mass of dust contained between the cylinders. This quantity is given by

$$q = \frac{\int dQ}{\int dm} = \frac{\int Q_m \, dm}{\int \zeta \, d\mathcal{T}}, \qquad (40)$$

where $d\mathcal{T}$ is the volume element per unit length, equal to $2\pi r dr$, and dm is the corresponding mass element $2\pi r \zeta \, dr$, when ζ, taken as a function of r only, is the mass of dust per unit volume of air. If ζ is assumed constant in the region between the cylinders, then from (35),

$$q = \left\{ \left[1/2(R^2 - r_o^2) \right] \cdot \left[3K/(K+2) \right] d_g^2 \, N \, e^{2(\ln \sigma_g)^2} \right\} \int_R^{r_o} E r dr. \qquad (41)$$

E as given by (39) must be inserted in (38) to evaluate C_o. This leads to an integral which may be evaluated with the aid of elliptic integral tables such as those of Byrd and Friedman (1954). However, it is adequate and much simpler for the present work to neglect the term $2pSr/3$ within the parentheses in (39). Hence, upon writing

$$E_o = (2i/k)^{\frac{1}{2}}; \quad A_o^2 = C_o k/2i, \qquad (42\ a,b)$$

(38) becomes

$$V = E_o \int_R^{r_o} (A_o^2 + r^2)^{\frac{1}{2}} dr/r. \qquad (43)$$

The integration leads to

$$(V/E_o) = (A_o^2 + r_o^2)^{\frac{1}{2}} - (A_o^2 + R^2)^{\frac{1}{2}}$$

$$+ (1/2)A_o \ln\left\{\left[(A_o^2+R^2)^{\frac{1}{2}}+A_o\right]\Big/\left[(A_o^2+R^2)^{\frac{1}{2}}-A_o\right]\right\}$$

$$+ (1/2)A_o \ln\left\{\left[(A_o^2+r_o^2)^{\frac{1}{2}}-A_o\right]\Big/\left[(A_o^2+r_o^2)^{\frac{1}{2}}+A_o\right]\right\}. \qquad (44)$$

If we set

$$x = r_o/A_o; \quad \xi = R/r_o; \quad \Lambda = V/E_o r_o, \qquad (45\ a,b,c)$$

then

$$\Lambda x = (1+x^2)^{\frac{1}{2}} - (1+\xi^2 x^2)^{\frac{1}{2}} - \ln \xi$$

$$+ \ln\left\{\left[(1+\xi^2 x^2)^{\frac{1}{2}}+1\right]\Big/\left[(1+x^2)^{\frac{1}{2}}+1\right]\right\}. \qquad (46)$$

It remains to determine x, which contains $A_o = (C_o k/2i)^{\frac{1}{2}}$, with Λ and ξ experimentally known. Equation (46) may be solved graphically from a plot of the right-hand member of (46) as a function of **x**. Then the intersection of a straight line through the origin with slope Λ determines x.

The quantity q can now be obtained by applying equation (41). We find

$$q = \left\{\left[1/2(R^2-r_o^2)\right] \cdot \left[3K/(K+2)\right] \ d_g^2 \ N \ e^{2(\ln \sigma_g)^2} \ E_o\right\}$$

$$\cdot \int_R^{r_o} (A_o^2 + r^2)^{\frac{1}{2}} \ dr/r. \qquad (47)$$

Upon neglect of r_o^2 compared with R^2, we may define

$$\chi = (1/2R^2) \ E_o \left[3K/(K+2)\right] \ d_g^2 \ N \ e^{2(\ln \sigma_g)^2}, \qquad (48)$$

and consequently,

$$q = \chi \int_R^{r_o} (A_o^2 + r^2)^{\frac{1}{2}}\, dr. \qquad (49)$$

Integration yields

$$(2q/\chi) = r_o(A_o^2 + r_o^2)^{\frac{1}{2}} - R(A_o^2 + R^2)^{\frac{1}{2}}$$
$$-(A_o^2/2)\ln\left\{ \left[(A_o^2 + R^2)^{\frac{1}{2}} + R \right] \Big/ \left[(A_o^2 + R^2)^{\frac{1}{2}} - R \right] \right\}$$
$$-(A_o^2/2)\ln\left\{ \left[(A_o^2 + r_o^2)^{\frac{1}{2}} - r_o \right] \Big/ \left[(A_o^2 + r_o^2)^{\frac{1}{2}} + r_o \right] \right\}, \qquad (50)$$

or

$$q = (\chi r_o^2/2x^2) \left\{ x(1 + x^2)^{\frac{1}{2}} - \xi x(1 + \xi^2 x^2)^{\frac{1}{2}} \right.$$
$$\left. -\ln \left[\left(\sqrt{1 + \xi^2 x^2} + \xi x\right) \Big/ \left(\sqrt{1 + x^2} + x\right) \right] \right\}. \qquad (51)$$

With x given by equation (46), q may be immediately calculated.

Measurement of Total Charge per Unit Mass of Dust

Theory of Measurement. The electrical charge Q_c on a system of known capacitance C may be determined by measuring the potential V, through the relation

$$Q_c = CV. \qquad (52)$$

Since the potential arises from an electrostatic charge, a low-drain instrument must be used. A vacuum-tube electrometer is convenient and has adequate charge sensitivity for the systems studied.

The system capacitance may be determined by measuring the rate of charge leakage through a known resistance R_g, as

shown in Figure 8. A charge is placed upon the system by contact with the battery (E) and a voltage reading is selected

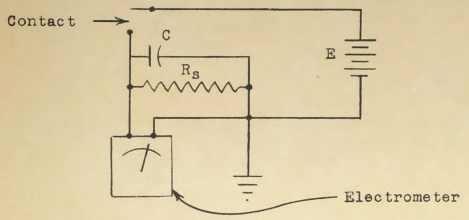

Figure 8. The charge leakage capacitance measurement circuit.

for time t equal to zero. A series of time-voltage readings are then taken as the charge decays through the resistance R_s. A straight line of slope $-1/R_sC$ should be obtained when the logarithm of voltage is plotted against time. The known resistance R_s must be large enough to allow timed measurements but small compared with the electrometer leakage resistance. C is then given by

$$C = t/R_s \ln (V_o/V_t), \qquad (53)$$

where V_o and V_t are potentials at t=0 and t=t respectively.

The Dust Charge Measurement Apparatus. Figure 9 is a schematic diagram of the dust charge measurement circuit, and the assembled apparatus is shown in Figure 10. A Keithley model 210 electrometer was used. Thin aluminum disks of 10.7 centimeters diameter were used for dust collection.

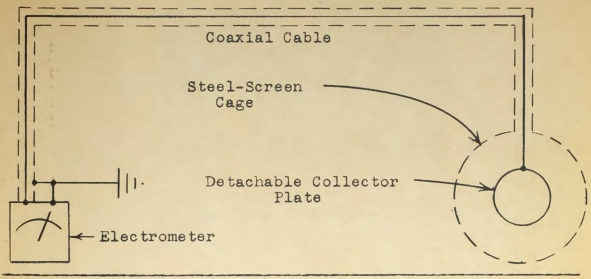

Figure 9. The dust charge measurement circuit.

To make a charge measurement a disk was clamped in place inside the steel-screen cage (see Figure 9), which shielded the disk from stray electric fields, but allowed dust to reach it. The cage was held in the dust cloud to collect a sample. After the potential was recorded, the disk was removed with tweezers, as shown in Figure 11, and the amount of dust collected was determined by weighing on an analytical balance.

The total charge per unit mass q was given by

$$q = Q_c/m_c, \tag{54}$$

where m_c is the mass of dust collected.

Experimental Investigation

An experiment was conducted to evaluate the reliability of the charge measurement method. Its results were compared

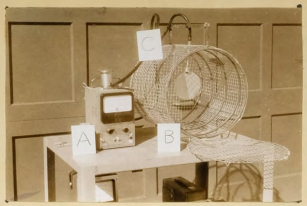

Figure 10. The charge measurement apparatus.

A. Electrometer.

B. Screen cage with disk in place.

C. Connecting coaxial cable.

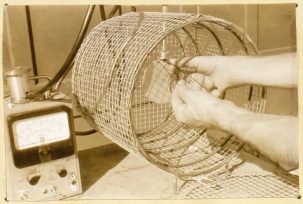

Figure 11. Removal of a dust-coated disk from the cage.

with those predicted by equation (51), and equation (41) with E assumed constant [see equation (56)].

Experimental Method

Apparatus. The laboratory chambers of the corona-discharge experiment were used. A concentric-cylinder ionizer with $r_o = 1.50 \times 10^{-2}$ cm., R = 3.65 cm., and a wire length of 25.4 cm. was used for dust charging. The wire was of solid steel; the outer electrode material was aluminum. The charger was operated at a positive potential of about 14 to 18 kv., with i held constant at 1.89×10^4 statcoulomb/cm.-sec.

A plane screen grid was placed normal to the axis of the charger at its outlet end. The grid was held at a positive potential of 10 kv. The positive grid, or "ion-trap", allowed the charged dust to pass, but prevented free air ions from reaching the collector disk and causing erroneous readings.

The collector-disk cage was located about two feet from the charger. It was placed away from the direct aerosol stream to prevent erosion of the dust deposit. Electrometer voltages were continuously recorded by a strip-chart recorder connected to the electrometer output. A schematic diagram of the apparatus is shown in Figure 12.

Procedure. Micronized talc dust with $d_g = 3.74\,\mu$ and $\sigma_g = 2.80$ was used. This dust material has a mass density $\epsilon = 2.8$ gm./cm^3 and a dielectric constant $K = 6.5$.

A series of dust exposures was given to each collector

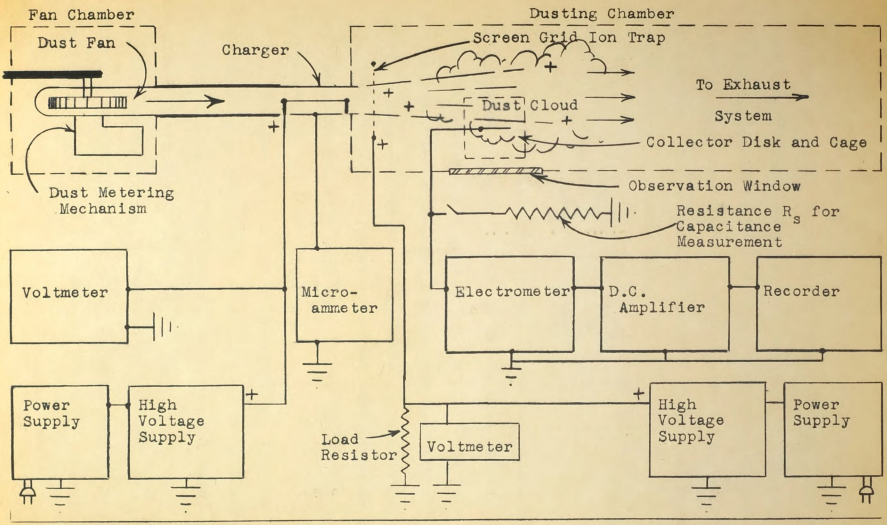

Figure 12. Schematic diagram for the charge measurement experiment.

disk. In this manner sufficient dust was accumulated to make the deposit weighing error small. The voltage V_γ was allowed to stabilize at each exposure, and then the charge was drained off through a known resistance, R_s. The latter procedure resulted in a decay curve on the strip-chart for capacitance determination. The quantity q was then calculated with a modified form of equation (54),

$$q = \left\{ \sum_{\gamma=1}^{n_o} C_\gamma / n_o \right\} \sum_{\gamma=1}^{n_o} V_\gamma / m_c, \qquad (55)$$

where n_o is the total number of exposures, C_γ is the measured capacitance at exposure γ, and m_c is the mass of dust collected.

Charge measurements were made at a dust feed rate of 0.641 gm./sec. and an average charger-air velocity of 915 cm./sec. These figures give a value for ζ of about 1.65×10^{-5} gm. dust/cm.^{3} of air. Twelve exposures were given to each disk. Measurements were made at relative humidities in the neighborhoods of 40 and 60 percent.

Positive-ion mobility data were obtained for the charger by the methods of the corona experiment. The data were corrected for air density variation and adjusted to give the accepted dry-air positive-ion mobility.

Since assumption of constant E in equation (41) leads to a trivial integration, E as given by equation (12) was inserted to obtain

$$q = (1/4)\left\{(2i/k)^{\frac{1}{2}}\left[3K/(K+2)\right]\ d_g^2\ N\ e^{2(\ln\sigma_g)^2}\right\} \qquad (56)$$

The ionic mobility information was used with equations (51) and (56) to obtain the approximate variation in the predicted q, as a function of relative humidity, for comparison with measured q values.

Discussion of Results

The charge measurement results and a plot of ionic mobility against relative humidity are given in Table IV and Figure A, respectively, of Appendix A. Results of q calculations using equations (51) and (56) appear in Table I of Appendix B.

The error in the average measured q_i values was estimated at about $\pm$ 6 to 8 percent, which agreed approximately with the standard error of the mean q_{av}, s, given by

$$s = \left\{\sum_{i=1}^{n}(q_{av} - q_i)^2/n(n-1)\right\}^{\frac{1}{2}}. \qquad (57)$$

The outer electrode of the charger invariably became heavily coated with dust during the exposure series with a given disk. Some systematic error in comparing the measured and calculated q values may be expected as a result. A slightly non-linear response of the recording system with respect to the electrometer was noted. This was an important error source in the capacitance measurement. It should have little effect upon the static voltage readings, since fre-

quent meter-recorder comparisons were made.

A sample graphical solution of equation (46) for x is given in Figure A of Appendix B. The measured and calculated q values are plotted as functions of relative humidity in Figure 13. The measured values were in general much higher than the calculated. The discrepancies are probably a result of lowered ionic mobilities in the presence of dust and impurities in the charger atmosphere. It is also possible that some additional charging effect may have existed in the vicinity of the ion trap. This could be tested by varying the ion trap potential.

Equations (51) and (56) predicted an increasing charge effect with increasing humidity, in direct opposition to the observations of this experiment and those of Hebblethwaite (1952). Figure B of Appendix B shows the predicted decrease in q as k increases.

The values for q predicted by equations (51) and (56) differ only slightly. This indicates that for some applications assumption of constant E in the interelectrode space would be an adequate approximation.

Conclusions

With careful instrumentation, the method of measuring charge will be quite satisfactory.

The theoretical charge equations do not account for reduction in charging effect with increasing humidity on the basis of ionic mobility. The shortcomings of the theory are

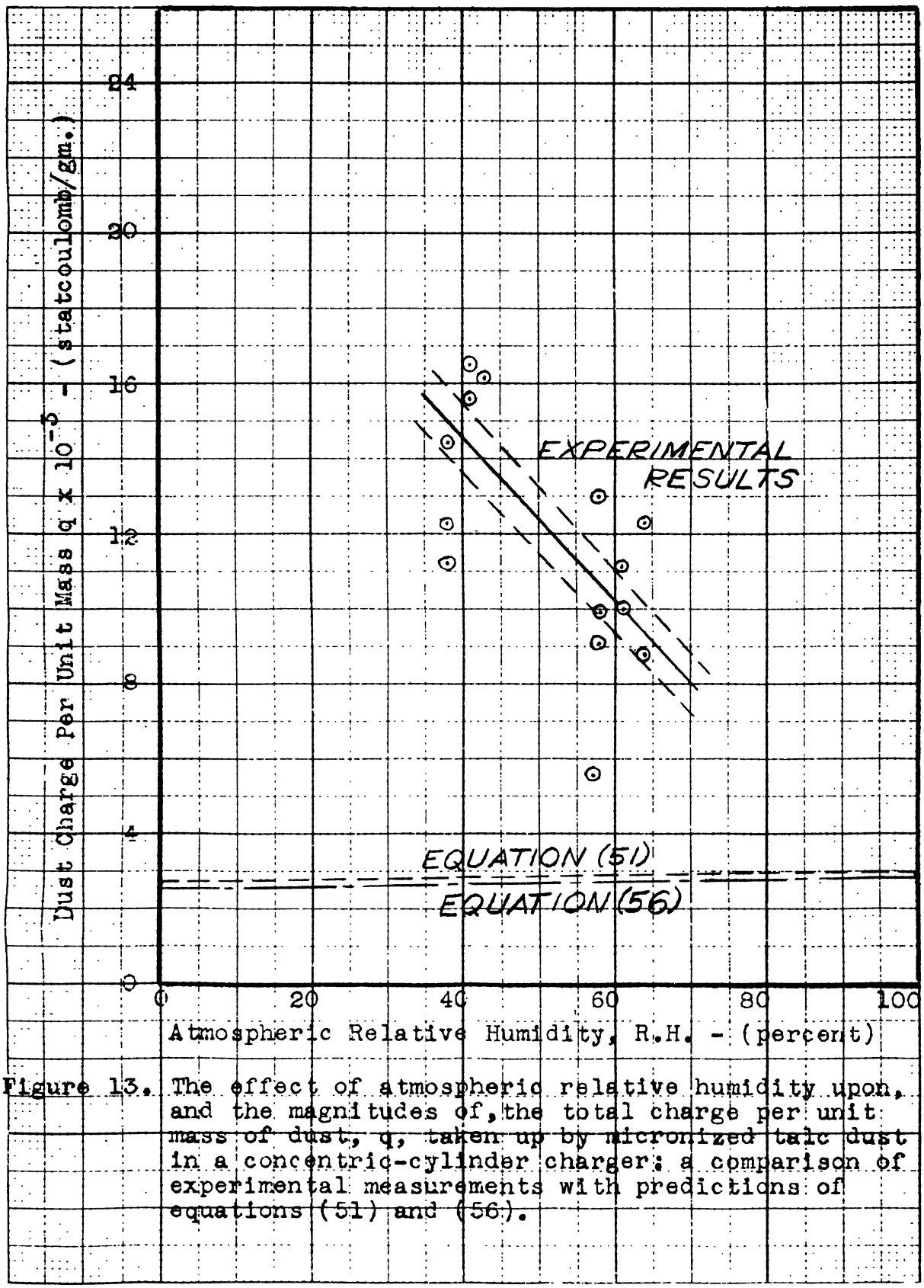

Figure 13. The effect of atmospheric relative humidity upon, and the magnitudes of, the total charge per unit mass of dust, q, taken up by micronized talc dust in a concentric-cylinder charger: a comparison of experimental measurements with predictions of equations (51) and (56).

probably in part attributable to its classical nature, apart from the more predominant effect of impurities in the inter-electrode space.

ANALYSIS OF A SEMICYLINDRICAL ELECTRIC FIELD FOR CHARGED DUST PRECIPITATION.

Ban (1955) performed laboratory experiments which indicated the effectiveness of an applied electric field for dust precipitation. The following study was undertaken to extend this concept to a semicylindrical field.

Preliminary Experimental Investigation

A preliminary study was conducted with rows of beans planted in field plots. This was a qualitative study of the applied field under conditions less favorable than previous laboratory tests. Attasorb dust with $d_g = 1.20\mu$, $\sigma_g = 2.27$ and $\epsilon = 2.45$ gm./cm.^{3} was used.

Equipment. A field crop duster supplied by Chemical Machines Limited of Winnipeg, Manitoba, Canada was used. It was fitted with a concentric cylinder charger having a wire length of 25.4 cm, a wire radius $r_o = 1.50 \times 10^{-2}$cm., and outer electrode radius R = 3.65 cm. Positive corona was employed throughout the test.

The electric field "hood" was of semicylindrical form, with a length of 107 cm. and radius of 21 cm. The material was galvanized steel sheet, and it was uninsulated except at the edges. The semicylinder potential was a positive 18 kv. The semicylinder was mounted so that it passed over

the plant row as the machine moved forward.

The duster is shown in Figure 14, and the position of the charger relative to the semicylinder is shown in Figure 15.

Procedure. Bean plant rows were dusted and operating characteristics of the semicylinder were qualitatively noted. The dust charge per unit mass q was determined by the charge-measurement method.

Results. In spite of the fact that the semicylinder was set close to the soil surface, slight air currents and the aerosol stream from the charger swept the dust cloud from the semicylinder before any appreciable precipitation could occur. It was impossible to hold the potential when the semicylinder touched the plants, which indicated that the plants act as grounded conductors under such circumstances. This observation was tested further with a bean plant set in a metal can. A charge placed on the plant by an ionized air stream could be held if the plant and container were isolated, but if the plant and container were grounded the charge was immediately lost.

Charge measurements gave $q = 4500 \pm 300$ statcoulombs/gm., with $V \simeq 14$ kv. and $i \simeq 189 \times 10^2$ statcoulombs/cm.-sec. at 50 percent relative humidity.

Theoretical Analysis of Dust Particle Behavior in the Semicylindrical Electric Field

General simplifying assumptions made are that the plant row may be represented by a semicylinder (concentric with

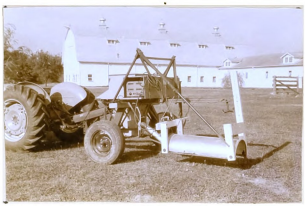

Figure 14. The Chemical Machines Ltd. duster. The conventional lateral dust distribution tubes were removed to allow mounting of the charger and semicylinder.

Figure 15. The dust charger and the semicylinder.

respect to the electric field semicylinder) and that the dust particles obey Stokes' law. Space charge is neglected so that the electric potential distributions satisfy Laplace's equation.

Analysis Assuming Concentric Cylinders of Infinite Extent. It is assumed that the problem may be represented by two concentric cylinders of infinite extent, as shown in Figure 16. This discounts edge effects, but greatly simplifies the analysis. The inner cylinder, r = a, represents the plant row at potential U(a) = 0, and the outer cylinder, r = b, represents the semicylinder at U(b) = V.

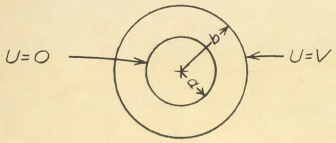

Figure 16. Representation of the applied field problem.

The potential distribution satisfies Laplace's equation,

$$\nabla^2 U = 0. \qquad (58)$$

If the potential is a function of r only, in cylindrical coordinates

$$\nabla^2 U(r) = (1/r)\left\{ d\left[r\, dU(r)/dr \right] \Big/ dr \right\} = 0. \qquad (59)$$

Integration of (59) yields

$$U(r) = C_1 \ln r + C_2, \qquad (60)$$

where C_1 and C_2 are integration constants. Insertion of the boundary conditions gives

$$U(r) = \left[V \ln(r/a)\right] / \ln(b/a). \qquad (61)$$

The electric field intensity vector, $\bar{E}$, is

$$\bar{E} = - \left[V/r \ln(b/a)\right] (\bar{r}/r). \qquad (62)$$

If the inner surface of the cylinder r = b is insulated by means of a dielectric K of thickness (b-h), then

$$U_1 = C_3 \ln r + C_4, \ (a \leq r \leq h), \qquad (63)$$

and

$$U_2 = C_5 \ln r + C_6, \ (h \leq r \leq b). \qquad (64)$$

At r = a, $U_1 = 0$; at r = h, $U_1 = U_2$ and $E_1 = K E_2$; at r = b, $U_2 = V$. The solutions are

$$U_1 = V \ln(r/a) \Big/ \left[(1/K)\ln(b/h) + \ln(h/a)\right], \ (a \leq r \leq h), \qquad (65)$$

$$U_2 = V \left\{1 - \left[(1/K)\ln(b/r)\right] \Big/ \left[(1/K)\ln(b/h)+\ln(h/a)\right]\right\}, \quad (h \leq r \leq b), \qquad (66)$$

$$\bar{E}_1 = - (V\bar{r}/r^2) \Big/ \left[(1/K)\ln(b/h)+\ln(h/a)\right], \ (a \leq r \leq h), \qquad (67)$$

and

$$\bar{E}_2 = -(V\bar{r}/Kr^2) \Big/ \left[(1/K)\ln(b/h)+\ln(h/a)\right], \ (h \leq r \leq b). \qquad (68)$$

Analysis Assuming Concentric Semicylinders of Infinite Extent. The problem may be represented as shown in Figure 17 (a), and solved by conformal mapping* as outlined by Churchill (1948). The solution is comparatively easy to obtain

---

*Kober (1957) gives many conformal representations useful in treating such problems.

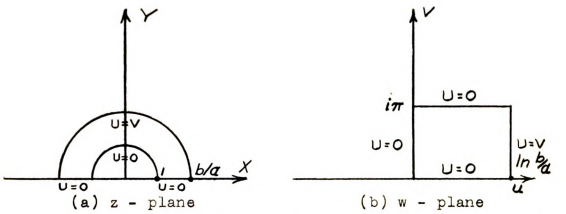

Figure 17.

for the region in the w - plane. This solution may be transformed to the z - plane by using the transformation $z = e^{w}$ to get

$$U = (4V/\pi) \sum_{n=1}^{\infty} \frac{(r/a)^{n'} - (r/a)^{-n'}}{(b/a)^{n'} - (b/a)^{-n'}} \cdot \frac{\sin n'\theta}{n'}, \quad (69)$$

where $n' = (2n-1)$, $1 \leq (r/a) \leq (b/a)$, and $0 \leq \theta \leq \pi$.

Estimation of Charge on a Particle of Given Radius. It is justifiable to assume a uniform surface charge density for dust on the basis of Ladenburg's (1930) equation (29) and experiments by Splinter (1955).

The particle surface area S_m per unit mass of dust material is given by Dallavalle (1943) as

$$\log S_m = \log (\alpha_s/\epsilon\alpha_v) - \log d_g - 5.757(\log \sigma_g)^2, \quad (70)$$

where α_s is the surface shape factor. For rounded particles

α_s/α_v is about 6.1; for "worn" particles, 6.4; for "sharp" particles, 7.0; for angular particles, 7.7; and for spheres 6. Then the charge per unit surface area Q_s is

$$Q_s = q/S_m. \tag{71}$$

Dallavalle gives the surface area Sp for a particle of diameter D as

$$S_p = \alpha_s D^2. \tag{72}$$

Hence, the estimated charge per particle q_o is

$$q_o = Q_s \alpha_s D^2. \tag{73}$$

Estimation of Time Required for a Charged Particle to Travel from the Outer to the Inner Cylinder. Stokes' law gives the limiting velocity v for a particle acted upon by a force F, and moving through a medium of viscosity η as

$$v = F/3\pi\eta D. \tag{74}$$

The particle will require a time $dt = dr/v$ to travel a distance dr. The total time required for the particle to travel from r = b to r = a is then, since $F = q_o E$ with E given by (62),

$$t = \int_b^a dr \Big/ \left[q_o^2/3\pi\eta D \right] = \left[3\pi\eta D \, (b^2-a^2) \ln(b/a) \right] \Big/ 2q_o V. \tag{75}$$

For air at 40°C $\eta = 1.918 \times 10^{-4}$ poise.

Ideally, a particle at r=b, in a plane normal to the axis of cylinders which contains the leading edge of the semi-cylinder has a time interval

$$t_1 = T/v_f \tag{76}$$

to reach r = a before the trailing edge passes the original

plane. Here Υ is the length of the semicylinder and v_f its uniform forward velocity. It is assumed that the particle remains in the original plane, which denotes a still medium. Equation (75) represents a limiting case, since a large proportion of the particles will require less time to reach the depositing region.

The Limiting Electric Potential V_c Required for Complete Precipitation in Still Air. Examination of equation (75) shows that $t \propto (1/D)$. Hence, to approach 100 percent depositing efficiency,

$$V_c = \left[3\pi\eta(b^2-a^2)\, v_f\, S_m \ln (b/a)\right] / 2q\, \alpha_s \Upsilon d_m, \qquad (77)$$

where d_m is the minimum diameter observed in particle size measurements.

Equation (77) is based on the simplification that the surface which encloses all particles approximates the lateral surface of a frustum of a cone of altitude Υ. The axis of the cone is imagined to coincide with that of the cylinders, with the periphery of its base of radius b containing the leading edge of the semicylinder. The other base is of radius a, with its periphery on the inner cylinder in the plane of the semicylinder trailing edge. The conic surface moves with the semicylinder. The actual case will vary from the above depending on air turbulence and the manner of introduction of dust, and should be accounted for with a more appropriate mathematical model.

The analysis serves to illustrate application of some of the theory, methods and information developed in the preceding investigations of this thesis.

GENERAL SUMMARY

The Parsons equation (1) is suitable for use in designing experimental cylindrical dust chargers. It provides an indirect means of measuring ionic mobilities through study of the concentric-cylinder corona discharge. A direct mobility measurement method, however, would be preferable for more accurate work.

Many of the ionic-mobility phenomena noted experimentally were explained in the light of modern gaseous electronics. The decrease in ionic mobility with increase in atmospheric relative humidity arises from the formation of cluster ions in the presence of the polar molecules of water vapor. The fact that negative air ions are more mobile than the positive is attributable to positive-ion aging effects and the non-existence of electron attachment to nitrogen molecules. The experimental variation of mobility with corona wire radius could not be explained, unless it perhaps arose from the classical nature of the Parsons equation.

The log-normal frequency distribution was shown to describe all particle size distributions studied.

The analytical and experimental methods of dust-charge determination were concluded to be satisfactory. However, the analytical expression does not explain the reduced charging effect at high humidity. Disagreement between

calculated and measured charges was attributed to greatly reduced ion mobilities in the presence of dust and impurities in the interelectrode space.

The usefulness of the measurement theory and methods developed was illustrated with a simple analysis of a semi-cylindrical precipitating field. To overcome strong influences of air currents, high though not impractical potentials would be required for its successful use. A much more detailed analysis would be necessary for proper estimation of the applied potential.

APPENDIX A

EXPERIMENTAL RESULTS

APPENDIX A

EXPERIMENTAL RESULTS

TABLE I

TABULATION OF DATA FOR EXPERIMENT ON CORONA DISCHARGE CHARACTERISTICS OF A WIRE COAXIAL WITH RESPECT TO A CYLINDER

Explanation of Symbols and Units.

1. r_o: Wire radius in centimeters.
2. R: Cylinder radius in centimeters.
3. R.H.: Relative humidity in percent.
4. i: Current per unit wire length in microamperes/centimeter.
5. V: Wire potential in kilovolts.
*6. C: Given in microamperes/centimeter-kilovolt.
*7. V_1, V_o: Given in kilovolts.
8. β: Factor in Equation (5) expressing enlargement of ionization region with increase of wire potential, given in centimeters/statvolt.
9. K: Apparent ionic mobility in $(\text{centimeters})^2/\text{statvolt-second}$.

* Parameters of Parson's equation (6).

* * *

Test 1.
$r_o = 6.82 \times 10^{-2}$ R = 1.90

R.H.	Positive Corona					
	21		64		92	
	i	V	i	V	i	V
	0.536	13.75	0.536	13.80	0.536	14.00
	1.292	14.00	1.292	14.00	1.292	14.15
	19.26	15.00	5.345	14.80	5.345	14.85
	30.95	15.75	11.63	14.85	11.63	14.90
	38.77	16.20	19.26	15.50	19.26	15.60
			30.95	16.30	30.95	16.40
			38.77	16.80	38.77	16.85

TABLE I Continued

Test 1 continued.

Positive Corona						
R.H.	21		64		92	
C	0.796		0.434		0.573	
V_1	17.2		16.9		17.4	
V_o	12.5		12.5		12.6	
	0.0146		0.0154		0.0144	
k	277		160		197	
Negative Corona						
R.H.	30		64		98	
	i	V	i	V	i	V
	0.536	13.50	0.536	14.00	0.536	12.05
	1.292	13.60	1.292	14.15	1.292	13.15
	19.26	14.70	19.26	14.80	19.26	14.20
	38.77	15.00	30.95	15.20	30.95	15.00
			38.77	15.50	38.77	15.45
C	0.650		0.581		0.704	
V_1	15.4		16.0		15.7	
V_o	13.1		13.0		12.3	
	0.0292		0.0227		0.0200	
k	453		316		338	

Test 2.

$r_o = 6.35 \times 10^{-3}$ R = 1.90

Positive Corona						
R.H.	42		65		97	
	i	V	i	V	i	V
	0.530	5.15	0.530	5.20	0.530	5.30
	1.278	5.65	1.278	5.70	1.278	5.85
	5.284	7.20	5.284	7.30	5.284	7.60
	11.50	7.30	11.50	7.50	11.50	7.70
	19.04	8.30	19.04	8.55	19.04	8.90
	30.60	9.65	30.60	9.80	30.60	10.30
	38.33	10.35	38.33	10.65	38.33	11.20

TABLE I Continued

Test 2 continued.

Positive Corona			
R.H.	42	65	97
C	1.99	1.78	2.05
V_1	13.5	13.1	15.2
V_o	3.67	3.76	3.67
	0.00111	0.00116	0.000944
k	568	532	497

Negative Corona						
R.H.	42		63		96	
	i	V	i	V	i	V
	0.530	5.05	0.530	4.90	0.530	4.55
	1.278	5.40	1.278	5.40	1.278	5.05
	5.284	6.65	5.284	6.80	5.284	6.80
	11.50	6.80	11.50	6.90	11.50	7.10
	19.04	7.40	19.04	7.80	19.04	8.05
	30.60	8.50	30.60	8.80	30.60	9.30
	38.33	9.00	38.33	9.35	38.33	10.15
C	1.34		2.09		2.63	
V_1	9.61		11.8		14.1	
V_o	3.87		3.89		3.46	
	0.00189		0.00137		0.00102	
k	652		735		692	

Test 3.

$r_o = 1.50 \times 10^{-2}$ R = 2.38

Positive Corona						
R.H.	32		63		93	
	i	V	i	V	i	V
	0.541	7.80	0.541	7.80	0.541	8.05
	1.302	8.30	1.302	8.35	1.302	8.65
	5.386	10.10	5.386	10.30	5.386	10.70
	11.72	10.30	11.72	10.45	11.72	10.95
	19.40	11.50	19.40	11.85	19.40	12.40
	31.19	12.10	31.19	13.50	31.19	14.20
	39.07	13.85	39.07	14.40	39.07	15.30

TABLE I Continued

Test 3 continued.

Positive Corona			
R.H.	32	63	93
C	1.38	0.630	1.18
V_1	16.1	14.2	18.3
V_o	6.44	6.94	5.90
	0.00235	0.00315	0.00184
k	551	337	370

Negative Corona						
R.H.	32		59		95	
	i	V	i	V	i	V
	0.541	7.80	0.541	7.55	0.541	7.15
	1.302	8.30	1.302	8.15	1.302	7.80
	5.386	9.85	5.386	9.80	5.386	9.90
	11.72	10.00	11.72	10.00	11.72	10.20
	19.40	10.90	19.40	11.05	19.40	11.50
	31.19	12.30	31.19	12.50	31.19	13.15
	39.07	13.00	39.07	13.35	39.07	14.20
C	1.44		0.842		1.45	
V_1	15.4		14.1		17.9	
V_o	6.40		6.91		5.44	
	0.00254		0.00315		0.00183	
k	622		451		452	

Test 4.

$r_o = 2.87 \times 10^{-2}$ R = 3.65

Positive Corona						
R.H.	27		61		96	
	i	V	i	V	i	V
	0.541	10.95	0.541	11.20	0.541	11.00
	1.302	11.80	1.302	12.15	1.302	12.00
	5.386	14.65	5.386	15.20	5.386	15.50
	11.72	15.05	11.72	15.50	11.72	15.45
	19.40	16.90	19.40	17.55	19.40	18.15
	31.19	19.30	31.19	20.15	31.19	20.90
	39.07	20.70	39.07	21.50	39.07	22.40

TABLE I Continued

Test 4 continued.

Positive Corona			
R.H.	27	61	96
C	1.04	0.977	0.991
V_1	25.9	27.2	29.4
V_o	8.46	8.35	8.04
	0.00239	0.00221	0.00195
k	522	450	404

Negative Corona					
R.H.	23		59		94	
	i	V	i	V	i	V
	0.541	10.80	0.541	11.05	0.541	10.35
	1.302	11.30	1.302	11.85	1.302	11.50
	5.386	13.50	5.386	14.70	5.386	15.00
	11.72	13.70	11.72	14.95	11.72	15.15
	19.40	15.20	19.40	16.65	19.40	17.20
	31.19	17.25	31.19	18.65	31.19	19.60
	39.07	18.60			39.07	20.35
C	0.889		1.07		0.912	
V_1	21.9		25.5		26.2	
V_o	7.99		8.48		7.69	
	0.00300		0.00245		0.00225	
k	556		550		429	

Test 5.

$r_o = 6.35 \times 10^{-3}$ R = 3.65

Positive Corona					
R.H.	36		61		97	
	i	V	i	V	i	V
	0.530	6.40	0.530	6.70	0.530	6.80
	1.278	7.45	1.278	7.85	1.278	8.15
	5.284	10.95	5.284	11.40	5.284	11.80
	11.50	11.25	11.50	11.65	11.50	12.00
	19.04	13.40	19.04	13.85	19.04	14.30
	30.60	16.15	30.60	16.65	30.60	17.05
	38.33	17.70	38.33	18.20	38.33	18.65

TABLE I Continued

Test 5 continued.

Positive Corona					
R.H.	36		61		97
C	2.06		1.90		1.79
V_1	28.6		28.9		30.0
V_o	4.24		4.40		4.47
k	0.000496		0.000493		0.000474
	966		881		802

Negative Corona						
R.H.	36		63		97	
	i	V	i	V	i	V
	0.530	6.35	0.530	6.35	0.530	6.20
	1.278	7.35	1.278	7.35	1.278	7.40
	5.284	10.40	5.284	10.70	5.284	11.15
	11.50	10.65	11.50	11.00	11.50	11.40
	19.04	12.65	19.04	13.20	19.04	13.60
	30.60	14.90	30.60	15.70	30.60	16.30
	38.33	16.20	38.33	17.15	38.33	18.00
C	1.81		1.64		2.18	
V_1	23.8		25.1		30.0	
V_o	4.36		3.93		4.16	
k	0.000623		0.000572		0.000467	
	1070		885		959	

Test 6.

$r = 6.82 \times 10^{-2}$ $R = 4.92$

Positive Corona						
R.H.	37		60		*	
	i	V	i	V	i	V
	0.542	18.30	0.542	19.15		
	1.306	19.50	1.306	19.95		
	5.400	20.70	5.400	23.30		
	11.75	20.80	11.75	20.80		
	19.46	22.20	19.46	22.20		
	31.27	23.45	31.27	23.35		
	39.17	24.45	39.17	24.50		

TABLE I Continued

Test 6 continued.

	Positive Corona		
R.H.	37	60	*
C	0.453	0.514	
V_1	25.4	24.9	
V_o	16.8	19.2	
	0.0102	0.0152	
k	736	1250	

	Negative Corona					
R.H.	35		60		*	
	i	V	i	V	i	V
	0.542	19.25	0.542	19.00		
	1.306	19.80	1.306	19.85		
	5.400	22.30	5.400	22.70		
	11.75	21.00	11.75	21.05		
	19.46	22.30	19.46	22.30		
	31.27	23.65	31.27	23.80		
	39.17	24.00				
C	0.515		0.499			
V_1	25.7		25.6			
V_o	18.4		18.4			
	0.0121		0.0123			
k	991		982			

*Data could not be obtained because of failure of the particular wire-cylinder combination to function satisfactorily at higher humidities.

TABLE I Continued

Test 7.

r_o= 1.50 x 10^{-2} R = 4.92

	Positive Corona					
R.H.	36		60		93	
	i	V	i	V	i	V
	0.522	10.10	0.522	10.10	0.522	10.50
	1.286	11.35	1.286	11.50	1.286	12.00
	5.157	15.80	5.157	16.15	5.157	16.95
	6.528	16.90	6.528	17.30	6.528	18.05
	13.06	21.15	13.06	21.65	13.06	22.80
	20.05	24.60	20.05	25.15	20.05	26.20
	26.57	27.60	26.57	28.45		
	29.86	29.45	29.20	29.55		
C	0.800		0.835		0.697	
V_1	42.1		48.4		44.0	
V_o	7.16		5.86		6.58	
	0.000746		0.000612		0.000695	
k	434		371		352	

	Negative Corona					
R.H.	41		58		93	
	i	V	i	V	i	V
	0.522	9.25	0.522	9.35	0.522	9.35
	1.286	10.80	1.286	10.85	1.286	11.00
	5.157	15.30	5.157	15.50	5.157	16.25
	6.528	16.40	6.528	16.50	6.528	17.40
	13.06	19.90	13.06	20.50	13.06	21.50
	16.76	21.65	15.85	21.80	14.46	22.15
C	0.601		0.660		0.530	
V_1	33.0		36.3		36.3	
V_o	6.03		5.32		5.42	
	0.000967		0.000841		0.000843	
k	422		403		324	

TABLE I Continued

Test 8.

r_o = 6.35 x 10-3 R = 4.92

Positive Corona

R.H.	38		61		96	
	i	V	i	V	i	V
	0.494	7.30	0.494	7.45	0.494	7.85
	1.216	8.80	1.216	9.10	1.216	9.60
	4.878	13.55	4.878	14.10	4.878	14.80
	6.175	14.70	6.175	15.35	6.175	16.00
	12.35	19.15	12.35	19.90	12.35	20.55
	18.96	22.70	18.96	23.60	18.96	24.20
	25.13	25.80	25.13	26.70		
	31.34	28.65				
C	1.81		1.05		0.956	
V_1	68.4		48.4		49.6	
V_o	3.32		3.90		3.92	
	0.000195		0.000285		0.000277	
k	605		512		455	

Negative Corona

R.H.	38		58		96	
	i	V	i	V	i	V
	0.494	7.30	0.494	7.15	0.494	7.10
	1.216	8.80	1.216	8.65	1.216	8.90
	4.878	13.40	4.878	13.55	4.878	14.30
	6.175	14.55	6.175	14.80	6.175	15.70
	12.35	18.30	12.35	18.85	12.35	19.80
	16.29	21.05	17.71	21.30	15.99	21.80
C	1.48		0.926		1.02	
V_1	56.5		41.1		46.4	
V_o	2.95		3.56		3.78	
	0.000237		0.000338		0.000298	
k	600		536		522	

TABLE II

PARTICLE SIZE MEASUREMENT DATA

	Dust					
	Attasorb		CCC Diluent*		Copper Sulfate**	
Particle Diameter Group (microns)	Number in Group	Percent Smaller Than Upper Limit	Number in Group	Percent Smaller Than Upper Limit	Number in Group	Percent Smaller Than Upper Limit
< 1.62	35	10.35	39	11.57	2	0.99
1.62- 3.24	264	88.46	181	65.28	62	31.53
3.24- 6.48	32	97.93	67	85.16	69	65.52
6.48- 9.72	7	100.00	13	89.02	36	83.25
9.72-12.96	0	----	25	96.43	13	89.65
12.96-16.16	0	----	5	97.91	9	94.08
16.16-19.44	0	----	5	99.39	6	97.04
19.44-32.40	0	----	2	100.00	4	99.01
>32.40	0	----	0	----	2	100.00
Total Particles Measured	338	----	337	----	203	----

* CCC Diluent is 97.73% calcium carbonate, with the remaining percentage consisting of miscellaneous compounds.

** This copper sulfate dust contained a small amount of inert ingredient.

TABLE III

GEOMETRIC MEAN PARTICLE DIAMETERS (d_g) AND GEOMETRIC STANDARD DEVIATIONS (σ_g) FOR SEVERAL DUSTS

Commercial Designation of Dust	Nature of Dust	d_g (microns)	σ_g
Attasorb	Micronized** clay	1.20	2.27
CCC Diluent	97.73% calcium carbonate	2.73	2.29
Copper Sulfate	Some inert ingredient present	4.65	2.26
Standard* Copper Sulfate	Some inert ingredient present	5.75	2.78
Micronized* Talc	Hydrated magnesium silicate	3.74	2.80

* From data obtained by Ban (1955).

** The term "micronized" indicates that the material has undergone a special fine grinding treatment.

TABLE IV

CHARGE MEASUREMENT DATA

Disk	Relative Humidity (Percent)	q (statcoulombs/gm.)
1	38	14400
2	38	11200
3	38	12300
4	41	15600
5	41	16500
6	42	16200
7	58	9020
8	57	5570
9	58	9970
10	61	11100
11	61	10000
12	58	13000
13	64	8790
14	64	12300
Averages	40	14600 ± 900
	60	10200 ± 820

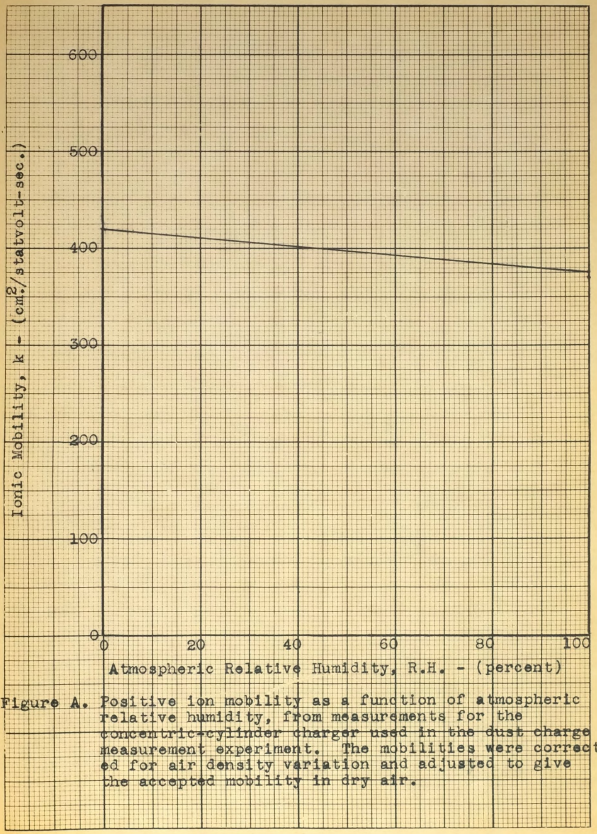

Figure A. Positive ion mobility as a function of atmospheric relative humidity, from measurements for the concentric-cylinder charger used in the dust charge measurement experiment. The mobilities were corrected for air density variation and adjusted to give the accepted mobility in dry air.

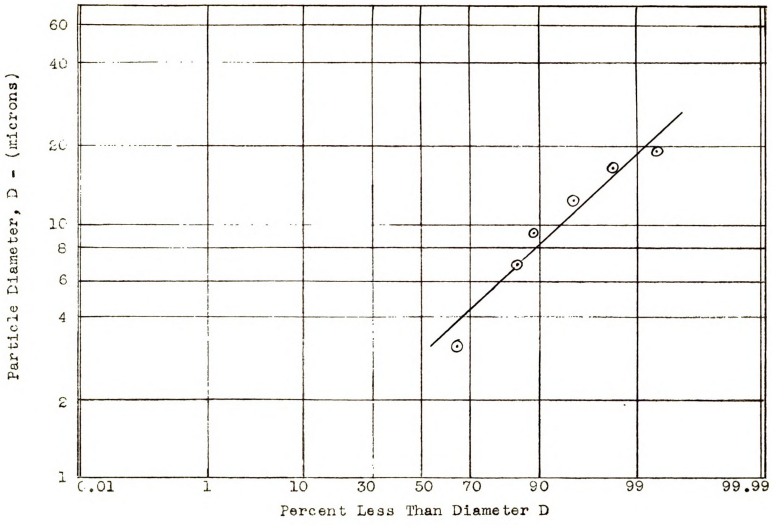

Figure B. A plot of dust particle diameters D against cumulative percentages of particles of size less than D for CCC Diluent Dust.

APPENDIX B

THEORETICAL RESULTS

TABLE I

CALCULATED VALUES FOR q

Dust: Micronized Talc.

Percent Relative Humidity	Equation (56)	Equation (51)	
	q*	x ($\times 10^2$)	q
0	2610	-3.54	2720
20	2650	-3.70	2720
50	2680	-3.85	2780
80	2730	-4.03	2820
100	2760	-4.23	2860

*q given in statcoulombs/gm.

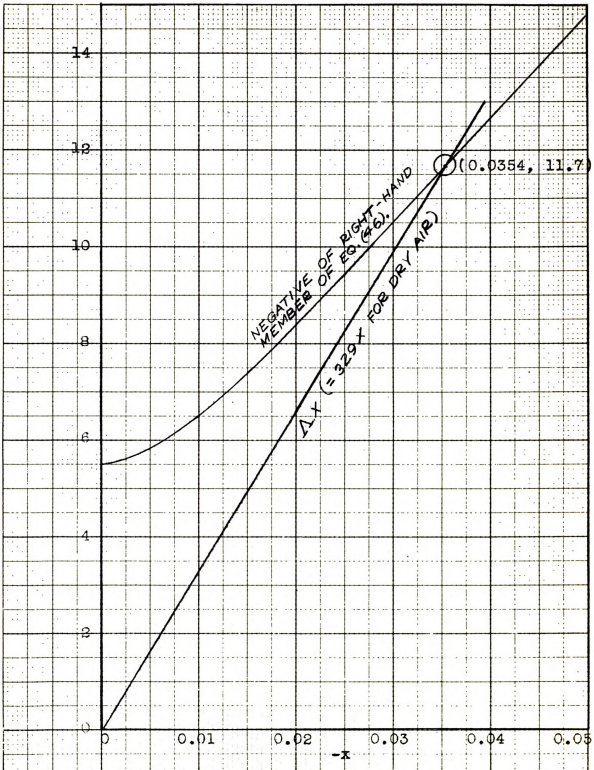

Figure A. Graphical solution of equation (46) for x under the conditions of the charge measurement experiment.

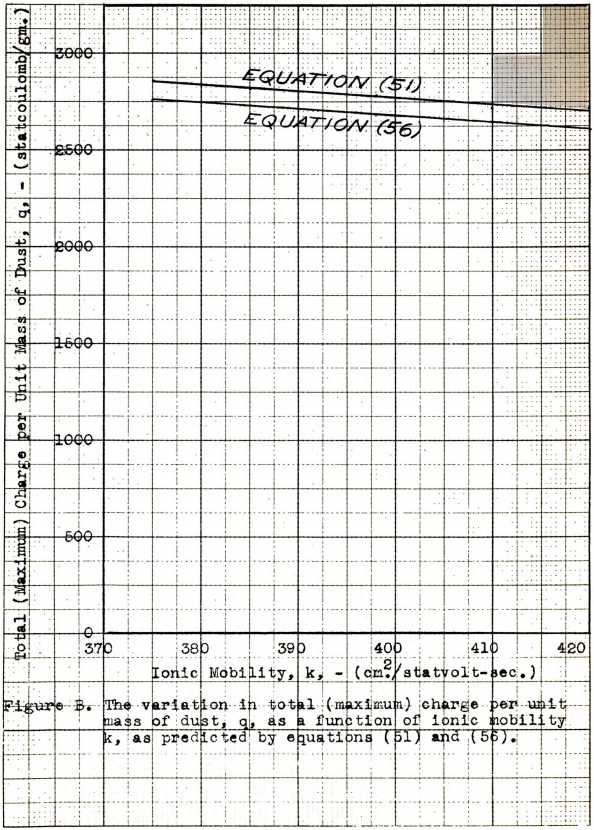

Figure 8. The variation in total (maximum) charge per unit mass of dust, q, as a function of ionic mobility k, as predicted by equations (51) and (56).

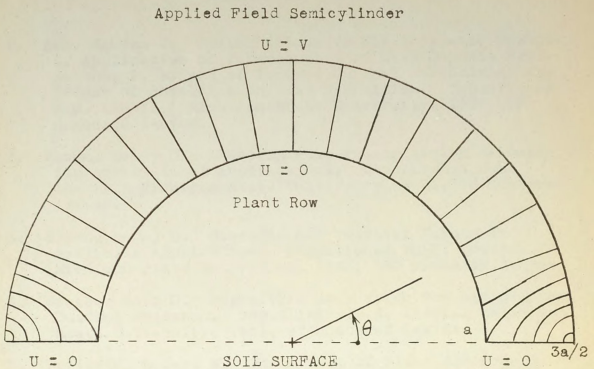

Figure C. A sketch of the electric field lines in the space between the field semicylinder and the plant row, based upon the solution (69) by conformal mapping.

REFERENCES CITED

1. Ban, Nguyen T. Contributions to Electrostatic Dusting: 1. Application of Polarography to Dust Deposit Evaluation, 2. Effect of Ionized Current Intensities and Effect of Shielding on Dust Deposition. Unpublished M.S. thesis. Michigan State University, 1955, 92 numbered leaves.

2. Bowen, Henry D. Electrostatic Precipitation of Dusts for Agricultural Applications. Unpublished M.S. thesis. Michigan State University, 1951, 76 numbered leaves.

3. Bowen, Henry D. Electric and Inertial Forces in Pesticide Application. Unpublished Ph.D. thesis. Michigan State University, 1953, 130 numbered leaves.

4. Brazee, Ross D. Deposition Evaluation For Agricultural Dusting Research. Unpublished M.S. thesis. Michigan State University, 1953, 97 numbered leaves.

5. Brittain, Robert W. The Effect of Plant Surfaces on Pesticidal Dust Deposition. Unpublished M.S. thesis. Michigan State University, 1954, 130 numbered leaves.

6. Byrd, Paul F., and Friedman, Morris D. Handbook of Elliptic Integrals for Engineers and Physicists. Springer-Verlag, Berlin, 1954, 355 pp.

7. Churchill, Ruel V. Introduction to Complex Variables and Applications. McGraw-Hill Book Company, Inc., 1948, 216 pp.

8. Cobine, James D. Gaseous Conductors. McGraw-Hill Book Company, Inc., New York, 1st ed., 1941, 606 pp.

9. Dallavalle, J. M. Micromeritics, the Technology of Fine Particles. Pitman Publishing Company, New York, 1943, 428 pp.

10. Fracker, S. B., and others. Losses in Agriculture. United States Department of Agriculture, June 1954, 190 pp.

11. Hampe, Pierre. Le Poudrage Electrostatique des Vegetaux. Reprint of the proceedings of a conference of La Ligue de Defense contre les ennemis des Cultures. Paris, 1947, 19 pp. Translated by Peter Hebblethwaite.

12. Hebblethwaite, Peter. The Application of Electrostatic Charging to the Deposition of Insecticides and Fungicides on Plant Surfaces. Unpublished M.S. thesis. Michigan State University, 1952, 117 numbered leaves.

13. Kober, H. Dictionary of Conformal Representations. Dover Publications, Inc., 2nd. ed., 1957, 208 pp.

14. Ladenburg, R. Untersuchungen uber die physikalischen Vorgange bei der sogenannten electrischen Gasreinigung: I Teil: Uber die maximale Aufladung von Schwebeteilchen. Annalen der Physik. 4(1930), pp. 863-897.

15. Loeb, Leonard B. Basic Processes of Gaseous Electronics. University of California Press, Berkley and Los Angeles, 1955, 1012 pp.

16. Lowe, H. J., and Lucas, D. H. The Physics of Electrostatic Precipitation. Static Electrification, British Journal of Applied Physics, Supplement No. 2, Institute of Physics, London, 1953, pp. 40-47.

17. Meek, J. M., and Craggs, J. D. Electrical Breakdown in Gases. Oxford University Press, London, 1953, 507 pp.

18. Parsons, Samuel R. The Current-Voltage Relation in the Corona. Physical Review. 5 (May 1924), pp. 598-607.

19. Smith, Richard K., and others. Agricultural Statistics-1954. United States Department of Agriculture, 1954, 607 pp.

20. Splinter, William E. Deposition of Aerial Suspensions of Pesticides. Unpublished Ph.D. thesis. Michigan State University, 1955, 164 numbered leaves.

21. Thomson, J. J., and Thomson, G. P. Conduction of Electricity Through Gases. Volume II. Cambridge University Press, London, 3d Edition, 1933, 608 pp.

22. Tyndall, A. M. The Mobility of Positive Ions in Gases. Cambridge University Press, London, 1938, 93 pp.

23. von Engel, A. Ionized Gases. Oxford University Press, London, 1955, 281 pp.